JMEPEG (2012) 21:1857–1861
DOI: 10.1007/s11665-011-0104-0

1059-9495/$19.00

High Speed Turning of H-13 Tool Steel Using Ceramics and PCBN

Usama Umer

(Submitted February 24, 2011; in revised form December 7, 2011)

H-13 is the toughest tool steel used in machined die casting and forging dies. Due to its extreme hardness and poor thermal conductivity high speed cutting results in high temperature and stresses. This gives rise to surface damage of the workpiece and accelerated tool wear. This study evaluates the performance of different tools including ceramics and PCBN using practical finite element simulations and high speed orthogonal cutting tests. The machinability of H-13 was evaluated by tool wear, surface roughness, and cutting force measurements. From the 2D finite element model for orthogonal cutting, stresses and temperature distributions were predicted and compared for the different tool materials.

Keywords finite element (FE), H-13, high speed turning

1. Introduction

High speed turning of hardened steel (hard turning) differs from conventional turning of softer materials in several key ways. Because the material is harder, specific cutting forces are larger than in conventional turning. At the small cutting depths required, cutting takes place on the nose radius of cutting tools, and the tools are prepared with chamfered or honed edges to provide a stronger edge geometry that is less prone to premature fracture. Cutting on a chamfered or honed edge equates to a large negative effective rake angle, while neutral or positive rake angles are typical in conventional machining. The large negative rake angles yield increased cutting forces compared to machining with positive rake tools, and also induce larger compressive loads on the machined surface (Ref 1).

Traditionally, a wide range of tool steels is used in producing machined dies and molds whereas hot work tool steels (the AISI H series) are generally the choice of material for die-casting and forging dies. AISI H-13 (chromium hot work steel) based dies withstand high process temperatures (315–650 °C) experienced in forging and die-casting and are usually in the hardness of 45–56 HRC (Ref 2). AISI H13 is the toughest of the conventional tool steels. Due to its extreme toughness and good red hardness, high speed cutting results in high temperatures and stresses at the cutting zone.

Ng and Aspinwall (Ref 3) observed three different types of chips when turning AISI H13 using PCBN tools. They are homogeneous deformed, inhomogeneous deformed and shear localized. Homogeneous deformed segmental chips only occurred when machining at 75 m/min with the 28 HRC workpiece and the chip grain structure was uniform. Inhomogeneous deformed segmental chips occurred at 150 m/min when machining the 42 HRC workpiece. The chips contained regions where deformation was very high and also relatively low. When the cutting speed was increased to 200 m/min, shear localized chips were produced with white layers along the gross fracture surface.

Continuous and serrated chip formation when machining AISI-H13 by PCBN was also simulated by Ng (Ref 4). Serrated chips were simulated using crack nucleation and growth module based on Johnson cook failure's criteria. However, both types of chips were simulated at the same cutting speed, and the transition from continuous to serrated with cutting speed was not presented.

This study aims to perform machinability analysis on H-13 with ceramics and PCBN using finite element simulations and high speed orthogonal cutting tests. The cutting forces obtained from finite element simulations were compared with experimental data to check its validity. The stress and temperature distributions from FE model along with experimental tool wear and surface roughness data were compared for each cutting tool material.

2. Experimental Setup

Orthogonal turning experiments were conducted with the same cutting parameters on hardened AISI H-13 tool steel tubes (50 HRC) using triangular tool inserts having a edge chamfer of 0.1 mm × 25°. Four types of tool materials were used including two PCBN and two ceramic inserts. The properties and composition of the workpiece and tool materials are listed in Table 1. Three cutting speeds of 150, 200, and 250 m/min were used. A constant feed rate of 0.25 mm/rev and depth of cut 2 mm were employed for all cutting force measurement. For tool wear and surface measurement, feed of 0.5 mm/rev and depth of cut of 0.5 mm were used. Cutting and thrust forces were measured, using a Kistler model 9257B force dynamometer. The force signals from the dynamometer fed into Kistler model 5017B dual-mode charge amplifiers. The analog force signals from the charge amplifier were then passed through a data acquisition card. A PC-based data acquisition program

Usama Umer, National University of Sciences and Technology, Islamabad, Pakistan. Contact e-mails: usama@pnec.edu.pk and usamaumer@yahoo.com.

Table 1 Composition and properties of PCBN and ceramic tools

	AISI H13	PCBN1	PCBN2	CERM1	CERM2
Composition (%)	C 0.32-0.42 Si 0.80-1.20 Cr 4.5-5.5	CBN 65, TiC 35	CBN 90, $AlB_2$10	Al_2O_3 70, TiCN 30	Al_2O_3 96, ZrO_2 4
Density (kg/m^3)	7800	4370	3399	4250	4020
Young's Modulus (GPa)	211	588	652	400	380
Poisson's ratio	0.280	0.171	0.128	0.194	0.210
Thermal conductivity (W/m/°C)	37	44	100	20	16
Specific heat (J/kg/°C)	560	750	960	748	600
Hardness (HRC*/HV)	49*	3500	4000	1930	1730

Fig. 1 Setup to analyze and record cutting forces data

(Dynoware) was used to acquire the sampled data and save for analysis. The setup is shown in Fig. 1.

A TIME GROUP TR 240 surface roughness tester with diamond stylus was used to measure surface roughness of workpiece. Flank wear was measured using optical microscope after every 4 min and the total machining time was 20 min.

3. Finite Element Model

ABAQUS/Explicit was utilized to model high speed turning operations. Continuous chip formation was assumed in this work. The FE model for continuous chip formation was based on the Lagrangian method. The workpiece was fixed and the cutting took place by the movement of the cutting tool. A chip separation criterion was adopted using the Johnson Cook shear failure model (Ref 4). For the workpiece, the Johnson and Cook constitutive model was used to include stress variations due to strain, strain rate, and temperature. This relationship is frequently adopted for dynamic problems with high strain rates and temperature effects.

$$\sigma = A + B\varepsilon^n \left[1 + C \ln\left(\frac{\dot{\varepsilon}}{\dot{\varepsilon}_o}\right)\right]\left[1 - \left[\frac{T - T_{\text{room}}}{T_{\text{melt}} - T_{\text{room}}}\right]^m\right] \quad \text{(Eq 1)}$$

where ε is the equivalent plastic strain, $\dot{\varepsilon}$ the equivalent plastic strain rate, $\dot{\varepsilon}_o$ is the reference strain rate and the operating temperature. The Johnson and Cook equation has five material constants, which are A yield stress constant, B strain hardening constant, n strain hardening exponent, C strain rate hardening constant, and m temperature dependency coefficient T_{room} and T_{melt} are room and melting temperatures and taken as 20 and 1480 °C, respectively. The material constants are determined from experiment results and can include data over a wide range of strain rates and temperatures. Due to the nonlinear dependence of the flow stress of the material during plastic strain, an accurate value of stress requires expensive iteration for calculation of the increment plastic strain. Johnson cook parameters values are shown in Table 2.

Table 2 The Johnson-Cook parameters for H-13

JC parameters	A	B	C	n	m
	674.8	239.2	0.056	0.44	2.7

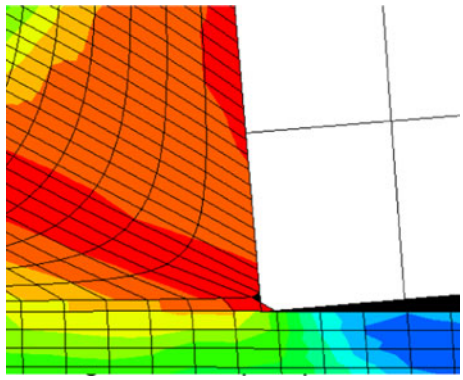

Fig. 2 Chip separation

The chip separation in the chip was simulated using Johnson and Cook damage law which takes into account strain, strain rate, temperature, and pressure (Ref 5). The damage was calculated for each element and is defined by

$$D = \sum \frac{\Delta\varepsilon}{\varepsilon_f} \quad \text{(Eq 2)}$$

where $\Delta\varepsilon$ is the increment of equivalent plastic strain during an integration step, and ε_f is the equivalent strain to fracture, under the current conditions. According to the feed rate tool passes through a series of elements as shown in Fig. 2. Upon penetration equivalent plastic strain of element increases and it is removed when incremental equivalent plastic strain is equal to strain at fracture, i.e., when $D = 1$. In fact, the element still exist, in order to keep the number of nodes,

elements and connectivities between nodes constant, but the deviatoric stress of the corresponding element are set to zero and remains zero for the rest of the analysis (Ref 5). The general expression for the fracture strain is given by

$$\varepsilon_f = (D_1 + D_2 \exp D_3\sigma^*)\left(1 + D_4 \ln\frac{\dot{\varepsilon}}{\dot{\varepsilon}_\circ}\right)\left[1 - D_5\left(\frac{T - T_{room}}{T_{melt} - T_{room}}\right)^m\right] \quad \text{(Eq 3)}$$

where $\dot{\varepsilon}_o$ is the reference strain rate and σ^* is the ratio of pressure stress to von-mises stress. D_1 to D_5 are material constants and determined by tensile and torsion tests. Numerical values used in the simulations are shown in Table 3.

When Zorev's sliding-sticking friction model is employed in the simulation, the division of the sliding and sticking regions is determined by two methods: one is to prescribe the length of each region, the other is to determine the sliding and sticking region automatically by a program according to a criterion (Ref 4), given by Eq 4

$$s = \mu p \quad \text{when } \mu p < \tau_{max} \quad \text{(Eq 4)}$$

$$s = \tau_{max} \quad \text{when } \mu p_{max}$$

where s, p, and τ are the friction, normal, and equivalent shear stress at the tool rake face. The second approach is adopted this analysis with a μ (coefficient of friction) value of 0.3.

A total of 4050 quadrilateral elements were designed on the workpiece and the cutting tool. In contrast to the experiments a sharp cutting tool was used in the FE model as shown in Fig. 3(a). FE simulations were carried out on a Celeron 2.4 GHz computer system with 248 MB RAM. The simulations required 10 to 15 CPU hours of computational time.

4. Results and Discussions

Figure 3(b) shows the deformed mesh after 0.8 ms of cutting time at speed of 200 m/min with PCBN1. The mesh at the tool cutting edge is heavily deformed as expected. The chip curled away from rake face at 0.62 mm to rake face length from the tool tip. The shear angle obtained from the simulation is 19.3° giving a resultant force of 1427 N.

Figure 4 details the resultant forces obtained by experiments and simulations for both types of cutting tools. It has been observed that higher forces are obtained with PCBN tools as compared to ceramics. This may be due to high thermal conductivities of the PCBN tools which infect lower the temperature at the shearing zone. Increase of cutting speed decrease the cutting forces for both types of cutting inserts. The decrease in cutting forces with cutting speed is higher for PCBN (5-7%) as compared to ceramics (3-4%). The figure also shows the forces obtained by finite element simulations. In general, FE results show similar trend as being observed with experimental data. This shows the model capability to predict machinability data for H-13 using advanced tool materials. However in almost all cases, FEM underestimates the cutting forces. The error is greatest at lowest cutting speed. This seems to be the result of unavailability of material's strain hardening and thermal softening data at elevated temperatures.

Figure 5 shows the temperature contours when machining H-13 with CERM2 and PCBN2 at speed of 200 m/min. Temperature at the tool-chip interface is much higher than at the primary shear zone. This is due to the fact that in addition to plastic deformation there is frictional work at the tool-chip interface. However, for the tool with highest thermal conductivity, i.e., PCBN2 the tool-chip interface temperatures are lower.

Table 3 The Johnson-Cook' Damage law parameters for H-13

JC parameters	D_1	D_2	D_3	D_4	D_5
	−0.8	2.1	−0.5	0.0002	2.7

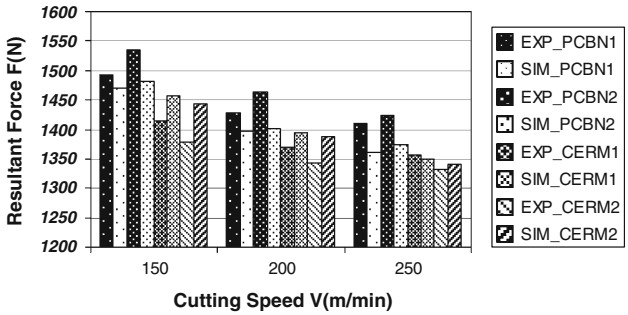

Fig. 4 Resultant forces obtained from experiments and simulations

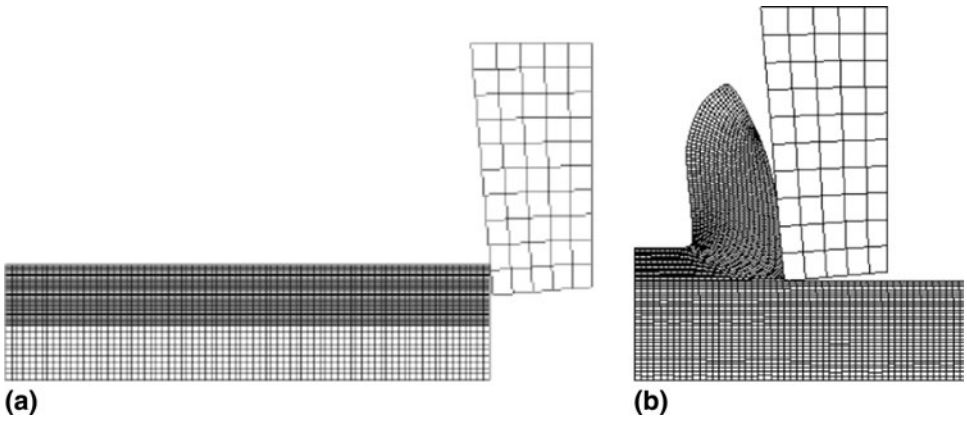

Fig. 3 Undeformed (a) and deformed (b) mesh of the workpiece and the cutting tool

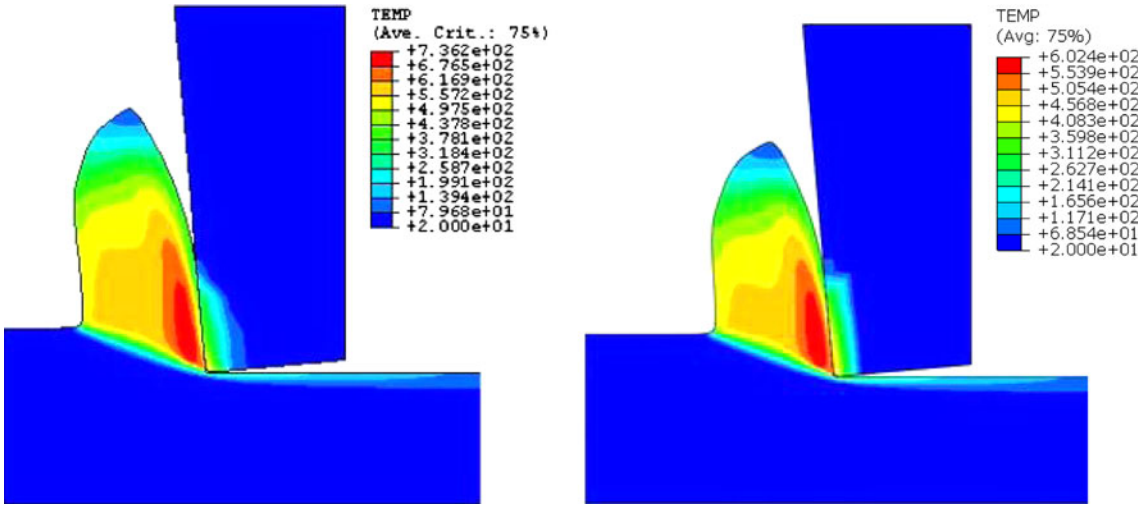

Fig. 5 Temperature contour (°C) when modeling with CERM2 (left) and PCBN2 (right) at speed = 200 m/min and feed = 0.25 mm/rev

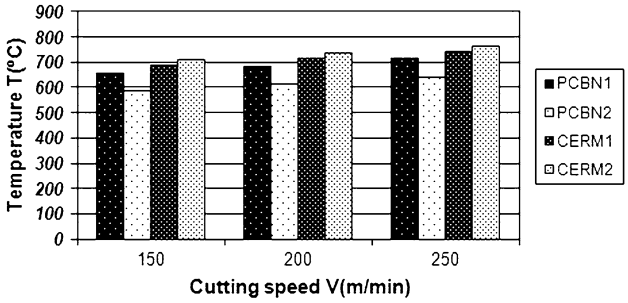

Fig. 6 Maximum temperatures obtained from experiments and simulations

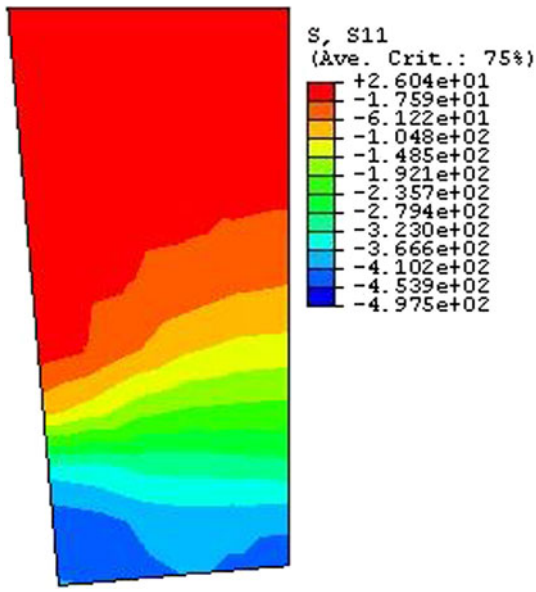

Fig. 7 Direct stresses (MPa) in the cutting direction for PCBN2

Figure 6 outlines the maximum temperatures obtained using both types of cutting tools. High temperatures are obtained when using ceramic tools in comparison to PCBN because of their low specific heats and thermal conductivities. As expected, CERM 2 shows the highest temperature and the lowest obtained with PCBN2. Similar results were found by Ng (Ref 6) when machining H-13 with PCBN. The temperature is increased with the increase of cutting speed for both types of cutting inserts. This is simply due to increase in the rate of plastic deformation.

The stresses on tool (PCBN2) in the cutting direction when machining at 200 m/min are shown in Fig. 7. Maximum compressive stress does not occur on the tool tip. This is due to the element deletion method; hence no load is acting on the tool tip. The stress field is compressive up to the point where the chip curls away from the tool rake face. The stress fields for both types of tools are similar, however they differ in magnitude. Due to high modulus of elasticity, PCBN2 shows highest stresses in the cutting direction.

Machinability of ceramics and PCBN were also analyzed using experimental flank wear and surface roughness data. Abrasive wear is usually a dominant wear mechanism on the flank face. Abrasion is characterized by development of grooves and ridges in the direction of tool sliding against a newly machined surface of the work piece or chip sliding against the rake face. The severity of abrasion can be increased in cases where the work piece materials contain hard inclusions, or when there is hard wear debris from the work piece or the tool at the interface. The abrasive wear in a ceramic cutting tool is related to its material properties, i.e., fracture toughness and hardness.

Figure 8 shows the flank wear versus cutting time curves for both types of cutting tools when machining at 200 m/min. PCBN tools show greater wear resistance due to their high hardness in comparison to the ceramic tools. Increase of the cutting speed increases the flank wear. This may be the result of increase in the abrasive action with the increase in cutting speed.

Surface roughness obtained using different cutting tools is shown in Fig. 9. Surface quality largely depends upon the accuracy of replication of cutting nose on the work surface. An ideal tool material is the one which can ensure high fidelity of its nose replication, thereby ensuring good control

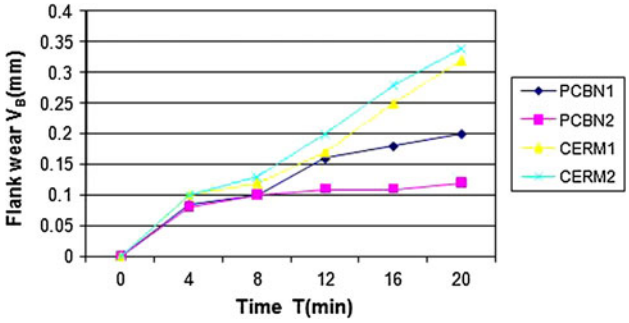

Fig. 8 Flank wear vs. time curve at speed = 200 m/min and feed = 0.5 mm/rev

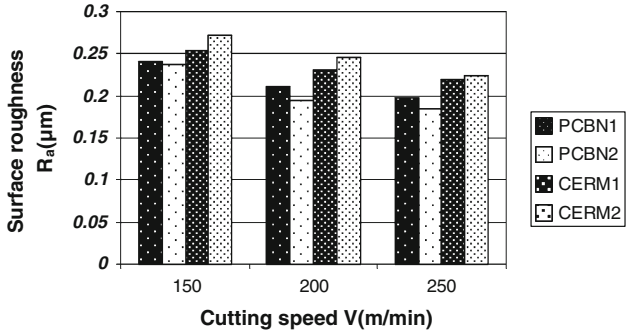

Fig. 9 Surface roughness obtained at different cutting speeds

over the surface quality (Ref 7). Similar to the results of flank wear, performance of PCBN tools is better than ceramics due to their high hardness and better stability of cutting nose.

5. Conclusions

1. The finite element model with the Lagrangian approach and element deletion technique can be used quite satisfactorily to predict workpiece machinability using different tools.
2. Ceramics cutting tools experienced low cutting forces in comparison to the PCBN tools.
3. The maximum temperature occurs at the chip tool interface and is higher for the ceramic tools.
4. The stress field is compressive up to the point where the chip curls away from the tool rake face.
5. PCBN tools show good flank wear resistance and obtained better surface finish than ceramic tools.

References

1. T.G. Dawson, "Machining Hardened Steel with PCBN tools", Ph.D. dissertation, Georgia Institute of Technology, 2002
2. T. Ozel and T. Altan, Process Simulation Using Finite Element Method-Prediction of Cutting Forces, Tool Stresses and Temperatures in High Speed Flat End Milling, *Int. J. Mach. Tools Manuf.*, 2000, **40**, p 713–738
3. E.G. Ng and D.K. Aspinwall, The Effect of Workpiece Hardness and Cutting Speed on the Machinability of AISI, H-13 Hot Work Die Steel when Using PCBN Tooling, *J. Manuf. Sci. Eng.*, 2002, **124**, p 588–594
4. E.G. Ng and D.K. Aspinwall, Modeling of Hard Part Machining, *J. Mater. Process. Technol.*, 2002, **127**, p 222–229
5. O. Pantale, J.L. Bacaria, O. Dalverny, R. Rakotomalala, and S. Caperaa, 2D and 3D Numerical Models of Metal Cutting with Damage Effects, *Comput. Methods Appl. Mech. Eng.*, 2004, **193**, p 4383–4399
6. E.G. Ng, D.K. Aspinwall, D. Brazil, and J. Monaghan, Modeling of Temperature and Forces when Orthogonally Machining Hardened Steel, *Int. J. Mach. Tools Manuf.*, 1999, **39**, p 885–903
7. S.A. Kumar, A.R. Durai, and T. SornaKumar, Machinability of Hardened Steel Using Alumina Based Ceramic Cutting Tools, *Int. J. Refract. Met. Hard Mater.*, 2003, **21**, p 109–117